Geophysical Research Letters

RESEARCH LETTER
10.1029/2022GL098860

Geomagnetic Activity Index Hpo

Y. Yamazaki[1], J. Matzka[1], C. Stolle[2], G. Kervalishvili[1], J. Rauberg[1], O. Bronkalla[1], A. Morschhauser[1], S. Bruinsma[3], Y. Y. Shprits[1,4,5], and D. R. Jackson[6]

[1]GFZ German Research Centre for Geosciences, Potsdam, Germany, [2]Leibniz Institute of Atmospheric Physics at the University of Rostock, Kühlungsborn, Germany, [3]CNES, Space Geodesy Office, Toulouse, France, [4]Institute of Physics and Astronomy, University of Potsdam, Potsdam, Germany, [5]Department of Earth and Planetary Sciences, UCLA, Los Angeles, CA, USA, [6]Met Office, Exeter, UK

Abstract The geomagnetic activity index *Kp* is widely used but is restricted by low time resolution (3-hourly) and an upper limit. To address this, new geomagnetic activity indices, Hpo, are introduced. Similar to *Kp*, Hpo expresses the level of planetary geomagnetic activity in units of thirds (0o, 0+, 1−, 1o, 1+, 2−, …) based on the magnitude of geomagnetic disturbances observed at subauroral observatories. Hpo has a higher time resolution than *Kp*. 30-min (Hp30) and 60-min (Hp60) indices are produced. The frequency distribution of Hpo is designed to be similar to that of *Kp* so that Hpo may be used as a higher time-resolution alternative to *Kp*. Unlike *Kp*, which is capped at 9o, Hpo is an open-ended index and thus can characterize severe geomagnetic storms more accurately. Hp30, Hp60 and corresponding linearly scaled ap30 and ap60 are available, in near real time, at the GFZ website (https://www.gfz-potsdam.de/en/hpo-index).

Plain Language Summary The geomagnetic activity index *Kp* is a measure of planetary geomagnetic activity, expressed in units of thirds (0o, 0+, 1−, 1o, 1+, 2−, …9o). *Kp* is widely used in the space physics community, as it is known to be a good proxy of the solar-wind energy input into the magnetosphere-ionosphere-thermosphere system. *Kp* has two important limitations. One is the temporal resolution. *Kp* is a three-hourly index, so that temporal features within 3 hr are not resolved. The other is the upper limit of the index. *Kp* does not exceed a maximum value of 9o, so that under extremely disturbed conditions, geomagnetic activity is not accurately represented. We introduce a group of new geomagnetic activity indices Hpo that overcomes these limitations. Hpo is designed to represent planetary geomagnetic activity in a similar way as *Kp* but with higher temporal resolution and without the upper limit at 9o. This paper describes the production of 30-min (Hp30) and 60-min (Hp60) indices, and demonstrates their properties in comparison with *Kp*. Hpo indices since 1995, including near-real-time values, are distributed through the GFZ website (https://www.gfz-potsdam.de/en/hpo-index).

Key Points:

- New *Kp*-like planetary geomagnetic activity indices, Hpo, are presented
- Hourly (Hp60) and half-hourly (Hp30) indices are available from GFZ website
- Hpo indices are open-ended without the upper limit at 9o

Correspondence to:

J. Matzka,
jmat@gfz-potsdam.de

Citation:

Yamazaki, Y., Matzka, J., Stolle, C., Kervalishvili, G., Rauberg, J., Bronkalla, O., et al. (2022). Geomagnetic activity index Hpo. *Geophysical Research Letters*, *49*, e2022GL098860. https://doi.org/10.1029/2022GL098860

Received 25 MAR 2022
Accepted 28 APR 2022

1. Introduction

Variations in the solar wind cause changes in electric currents that flow in the magnetosphere and ionosphere. The associated changes in the magnetic field can be observed using magnetometers on the ground. There exist various types of geomagnetic indices to monitor the intensity of geomagnetic disturbance associated with solar wind variations (Mayaud, 1980). The *Kp* index is one of the most widely used indices of geomagnetic activity. The derivation, application and historical background of *Kp* are detailed in Matzka, Stolle, et al. (2021), and thus are described here only briefly.

Kp is derived from *K* indices (Bartels et al., 1939) evaluated at 13 subauroral observatories from both northern and southern hemispheres. A *K* index expresses geomagnetic activity on a scale of 0–9 at each observatory for a given 3-hourly interval of the UT day (00–03, 03–06, …, 21–24 UT). It is based on the range of geomagnetic disturbance over the 3-hourly interval, which may contain geomagnetic pulsations (McPherron, 2005; Saito, 1969), bays associated with substorms (McPherron, 1970; Lyons, 1996), sudden storm commencements and sudden impulses (Araki, 1994), geomagnetic storm main phase (Gonzalez et al., 1994) and solar-flare and eclipse effects (Yamazaki & Maute, 2017). *K* is designed to have a similar frequency distribution regardless of observatory, and thus it does not depend on latitude. *K* indices are converted to standardized *Ks* indices, which take into account the influence of seasonal and UT biases. *Kp* is the average of the 13 *Ks* indices expressed in units of thirds (0o, 0+, 1−, 1o, 1+, 2−, …, 9o), thus it represents planetary, rather than local, geomagnetic activity. The complete time series of the definitive *Kp* index since 1932 and nowcast indices for the most recent hours

are available from the *Kp* website at Deutsches GeoForschungsZentrum GFZ (https://www.gfz-potsdam.de/en/kp-index/) with a digital object identifier (DOI; Matzka, Bronkalla, et al., 2021). Real-time *Kp* forecasts (Shprits et al., 2019) based on solar wind data are also available from the GFZ website (https://spaceweather.gfz-potsdam.de/products-data/forecasts/kp-index-forecast).

The *Kp* index has a wide range of applications in space physics studies. For example, *Kp* can be used to select undisturbed data from the measurements obtained from the magnetosphere, ionosphere or thermosphere to determine their climatological base states (e.g., Drob et al., 2015; Fejer et al., 2008). *Kp* is also often used for modeling the geospace response to solar wind variations. Just to give a few examples, *Kp* is used to drive the 3-D Versatile Electron Radiation Belt model (Subbotin et al., 2011), the Whole Atmosphere Community Climate Model with thermosphere and ionosphere extension (WACCM-X; Liu et al., 2018) and the Naval Research Laboratory Mass Spectrometer Incoherent Scatter radar empirical atmospheric model (Emmert et al., 2021), among many other models of the magnetosphere, ionosphere and thermosphere. Thomsen (2004) argued that what makes *Kp* so useful is its sensitivity to the latitudinal distance from the *Kp* stations to the equatorial edge of auroral currents, which is tightly linked to the strength of magnetospheric convection.

Kp has two important limitations. One is the temporal resolution. *Kp* cannot resolve temporal features within 3 hr. For example, the onset of geomagnetic disturbance determined by *Kp* could be off from the actual onset by up to 3 hr. This could be an issue when *Kp* is used to drive a geospace model, because the state of the magnetosphere, ionosphere and thermosphere can change significantly within the 3-hr interval. As a compromise, some models use interpolated *Kp* values as input data, for example, thermospheric density models (Vallado & Finkleman, 2014), WACCM-X (Liu et al., 2018). The other limitation of *Kp* is its upper limit at 9o. *Kp* is not able to quantify geomagnetic activity after it reaches 9o. Extreme geomagnetic storms involving $Kp = 9o$ are not necessarily equally strong in terms of geomagnetic disturbance. Extrapolated values of *Kp* above 9o are sometimes used for a better representation of geomagnetic activity during severe geomagnetic storms (e.g., Shprits et al., 2011).

The objective of this paper is to introduce a new group of *Kp*-like geomagnetic indices. The indices are collectively called Hpo, where "H" stands for *half-hourly* or *hourly*, "p" for *planetary*, and "o" for *open-ended*. Hpo has been conceived and developed under the EU Horizon 2020 project, Space Weather Atmosphere Model and Indices (SWAMI; Jackson et al., 2020). Hpo is designed to represent planetary geomagnetic activity in a similar manner as *Kp* but with higher time resolution and without an upper limit, to overcome the limitations of *Kp* described above. The derivation of 30-min (Hp30) and 60-min (Hp60) indices is outlined in Section 2, and their basic properties are described in Section 3.

2. Derivation of Hpo

Hpo indices are derived using 1-min magnetic data from the same 13 subauroral observatories as *Kp* (see Section 2.2 of Matzka, Stolle, et al., 2021). Time series of Hpo starts from the year 1995, because 1-min digital data are not available from all the observatories before 1995. The procedure for deriving Hpo is similar to that for nowcast *Kp* described in Matzka, Stolle, et al. (2021), involving the steps described below.

2.1. Evaluation and Removal of Quiet Curve

Records of the geomagnetic field from a ground station contain regular quiet daily variation and geomagnetic disturbance (Chapman & Bartels, 1940). The estimation of the quiet curve for Hpo is based on the Finnish Meteorological Institute method (Sucksdorff et al., 1991), which uses 1-min data from the previous day, present day, and subsequent day. The quiet curve is obtained for the northward *X* and eastward *Y* components of the geomagnetic field, and subtracted from the corresponding data, which leaves geomagnetic disturbance.

2.2. Evaluation of the Magnitude of Geomagnetic Disturbance

The magnitude of geomagnetic disturbance is evaluated for every 30-min interval for Hp30 and 60-min interval for Hp60. For a given time interval, the range of geomagnetic disturbance (i.e., maximum minus minimum value) is compared with the maximum absolute value of geomagnetic disturbance, and the larger value of the two is adopted as the magnitude of geomagnetic disturbance. This contrasts with the derivation procedure for *Kp*, which always uses the range of geomagnetic disturbance. We found that this modification of the procedure improves

Table 1
Lower Limits of H30, H60, and K for the Niemegk Observatory

Index	0	1	2	3	4	5	6	7	8	9
H30 (nT)	0	2.16	4.46	8.89	17.9	33.9	65.7	119	190	267
H60 (nT)	0	2.97	6.11	12.1	24.3	44.7	82.7	144	218	337
K (nT)	0	5.00	10.0	20.0	40.0	70.0	120	200	330	500

the compatibility between Hpo and *Kp*. The magnitude of geomagnetic disturbance is obtained for the *X* and *Y* components, and the larger value is used in the next step.

2.3. Evaluation of H30 and H60 Indices

H30 and H60 indices are analogous to *K* indices for *Kp*, and are collectively called H herein. For the evaluation of *K*, an observatory-specific table is used for converting the magnitude of geomagnetic disturbance (in nT) to an integer *K* value (0–9). An example of the conversion table for the Niemegk observatory can be found in Table 1. New tables have been created for each observatory that convert the magnitude of geomagnetic disturbance to an H value (0–9). This was done, for each observatory, by generating a conversion table for H in such a manner that the frequency distribution of H is as similar as possible to the frequency distribution of *K*. The construction of the conversion tables for H is based on the geomagnetic data during 1995–2017, which were all the available data when the construction of Hpo was initiated. The conversion table for H30 and H60 for Niemegk is presented in Table 1. Furthermore, extended conversion tables are produced in order to allow H to go beyond 9. In the extended conversion tables, the maximum value of H is unlimited. The lower limit for H = 10 is given by the lower limit of H = 9 multiplied by a factor of 1.35. The lower limit of H = 11 is given by the lower limit of H = 10 multiplied by a factor of 1.30, and the lower limit of H = 12 is given by the lower limit of H = 11 multiplied by a factor of 1.20. For values of H greater than 12, the multiplication factor will be always 1.20, so that H can be defined no matter how large the magnitude of geomagnetic disturbance is. These multiplication factors were determined on a trial-and-error basis so that the behavior of the final Hpo index above 9o will be compatible with those of other open-ended indices (see Section 3).

2.4. Evaluation of Hp30 and Hp60 Indices

H indices are converted to standardized H*s* indices using the same method for converting *K* to *Ks*. The conversion tables can be found in the Supporting Information of Matzka, Stolle, et al. (2021). The conversion of H to H*s* minimizes the influence of seasonal and UT biases. Finally, the average of the 13 H*s* indices is converted into Hpo values in units of thirds (0, 1/3, 2/3, 1, 4/3, 5/3, 2, …) in analog fashion as with the nowcast *Kp* (see Section 3.3 of Matzka, Stolle, et al., 2021) and expressed as (0o, 0+, 1−, 1o, 1+, 2−, …) following the convention for *Kp*. The Hpo value is derived using the H indices evaluated with the conversion tables capped at 9 (like the one shown in Table 1). If this initial Hpo value is 9o, all the H indices are re-evaluated using the extended conversion tables, in which H can go beyond 9, to re-calculate Hpo. This ensures that Hpo and *Kp* behave similarly up to 9− (and differently only at 9o and above).

Like *Kp*, Hpo indices are a quasi-logarithmic, rather than linear, measure of geomagnetic activity, and thus are not suitable for basic arithmetic operations such as addition and multiplication. To avoid this issue, linearly scaled ap30 and ap60 indices (collectively called apo) are produced for Hp30 and Hp60, respectively, by using the table that is used for producing *ap* from *Kp* (Matzka, Stolle, et al., 2021) but extending its higher end in a similar manner as the extension of H tables above 9. The relationship between Hpo and apo is illustrated in Figure 1a. Like *ap*, values of apo correspond to half the magnitude of geomagnetic disturbance at Niemegk.

Hp30 and Hp60, along with their corresponding ap30 and ap60, are archived since 1995 and available, in near real time, from the GFZ website (https://www.gfz-potsdam.de/en/hpo-index) with DOI (https://doi.org/10.5880/Hpo.0002) under the CC BY 4.0 license (Matzka et al., 2022, for data publication).

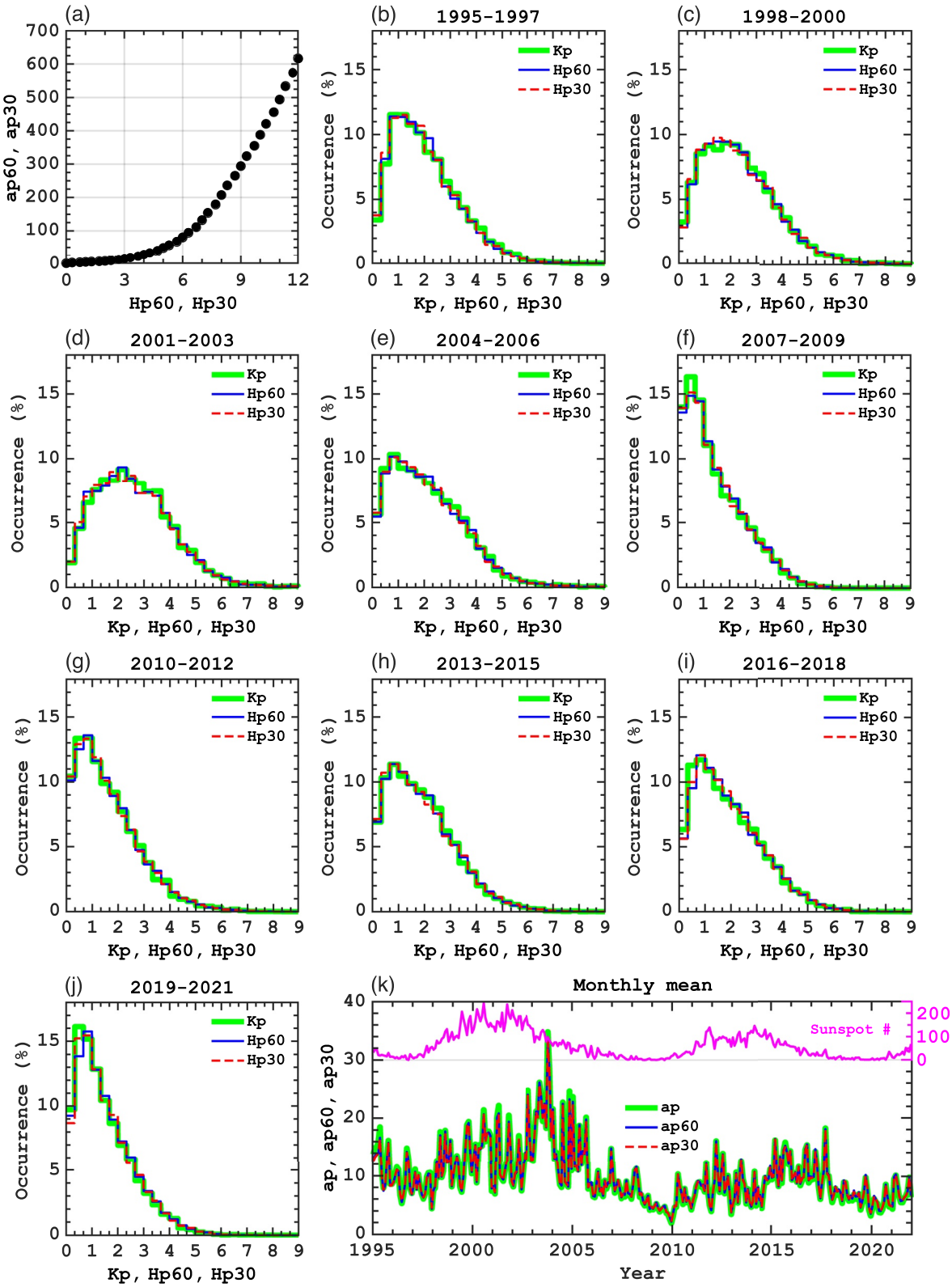

Figure 1. (a) The relationship between Hpo and apo. (b–j) Frequency distributions of the occurrence of *Kp*, Hp60, and Hp30 values for different years. (k) Monthly mean values of *ap*, ap60, and ap30 during 1995–2020. The total sunspot number is also indicated.

3. Some Properties of Hpo

The frequency distributions of the occurrence of Hp30, Hp60, and *Kp* values are compared in Figures 1b–1j for every 3-year interval from 1995 to 2021. The distribution pattern of *Kp* is different in different solar cycle phases. For instance, during the solar minimum years 2007–2009 (Figure 1f) and 2019–2021 (Figure 1j), the occurrence rate of low *Kp* values (e.g., $Kp \leq 1o$) is appreciably higher than during the solar maximum years 2001–2003 (Figure 1d) and 2013–2015 (Figure 1h). Hp30 and Hp60 reproduce different distribution patterns of *Kp* well, even for the later years not used in the construction of the conversion tables defining the H indices. The agreement of Hp30 and Hp60 with *Kp* during 2018–2021 (Figure 1j) suggests that the conversion tables for H indices are valid beyond the period 1995–2017.

The linearly scaled ap30 and ap60 indices are suitable for assessing average geomagnetic activity over a certain period. Monthly mean values of ap30 and ap60 are plotted in Figure 1k. They are in good agreement with monthly mean *ap*, showing 11-year solar-cycle variation. The sunspot number is also displayed in Figure 1k for comparison. Geomagnetic activity is known to be highest during the declining phase of solar cycle due to the effects of recurrent high speed solar wind streams (Lockwood et al., 1999).

In Figure 2, Hp30 (top), Hp60 (middle), and *Kp* (bottom) are compared with other geospace indices. The left panels show comparisons with Newell's coupling function (Newell et al., 2007), which is a measure of the energy input from the solar wind into the magnetosphere. The coupling function was derived using OMNI 5-min solar wind data (King & Papitashvili, 2005). Panels in the middle and right columns show comparisons with AE and PC indices, respectively. The AE index is a measure of auroral electrojet activity based on geomagnetic field measurements in the auroral region. The PC index represents geomagnetic activity in the polar region (Troshichev et al., 1988). Following Stauning (2007), the average of the PC indices from the northern (PCN) and southern (PCS) hemispheres were calculated using non-negative values. For comparisons with Hpo and *Kp* indices, 5-min solar wind data and 1-min AE and PC indices were averaged over every 30-min intervals. Hp60 and *Kp* are assumed to remain the same within their temporal windows. The solar wind data were shifted by 20 min to account for the delay due to energy transfer from the bow shock to the ionosphere (Manoj et al., 2008).

The solar-wind coupling function, AE and PC indices averaged at each value of Hpo and *Kp* from 0o to 9− are indicated in Figure 2 by black dots, with error bars representing the standard deviation. Curves in green show the best-fitting third-degree polynomial function for Hpo and *Kp* below 9o. The fitted curves for Hp30, Hp60, and *Kp* are similar to each other. The results suggest that for Hpo <9o, the dependence of Hp30 and Hp60 on the solar-wind coupling function, AE and PC indices is consistent with that of *Kp*. For Hpo ≥9o, the number of data points is rather small, and thus the average solar-wind coupling function, AE and PC indices were not calculated for each Hpo value. Instead, a single average value was derived using all the data corresponding to Hpo ≥9o (gray dots), which is indicated by the yellow dot in each panel of Figures 2a–2f. It is seen that the average value falls near the polynomial curve derived from the data for Hpo <9o. The results suggest that Hp30 and Hp60 can represent geomagnetic activity for Hpo ≥9o in the manner expected from their behavior for Hpo <9o.

The behavior of Hpo at its high end is further illustrated in Figure 3 based on five geomagnetic storm events. The selected geomagnetic storms are those in November 2003, March 2001, October 2003, November 2004, and July 2002, which are the five most intense geomagnetic storms during the period considered in this study (1995–2021) according to the minimum value of the Dst index. The left panels show time series of Hp30, Hp60, and *Kp*, as well as the Dst index, over a 7-day interval, in which the third day corresponds to the storm main phase. The temporal evolution of *Kp* is generally well captured by Hp30 and Hp60. Variations within 3 hr are seen in Hp30 and Hp60, which are not resolved by *Kp*. The maximum values of Hp30, Hp60, *Kp*, and the minimum value of Dst are (9−, 9−, 9−, and −422) for the November 2003 event, (10o, 10−, 9−, and −387) for the March 2001 event, (12−, 12−, 9o, and −383) for the October 2003 event, (11−, 9−, 9−, and −374) for the November 2004 event and (11o, 11o, 9o, and −300) for the July 2002 event. Thus, according to Hpo, the October 2003 event is the strongest among the five. Hpo ≥9o is seen mainly during the storm main phase, when the Dst index rapidly decreases. The right panels compare the 3-hourly mean of Hp30 (calculated from ap30) and *Kp*. The correlation is rather good; the correlation coefficient *r* is greater than 0.98 in all cases. Similarly good correlation is found for the comparison between 3-hourly mean of Hp60 and *Kp* (not shown here). These results suggest that Hpo can represent geomagnetic activity in a similar way as *Kp* even during the strongest geomagnetic storms.

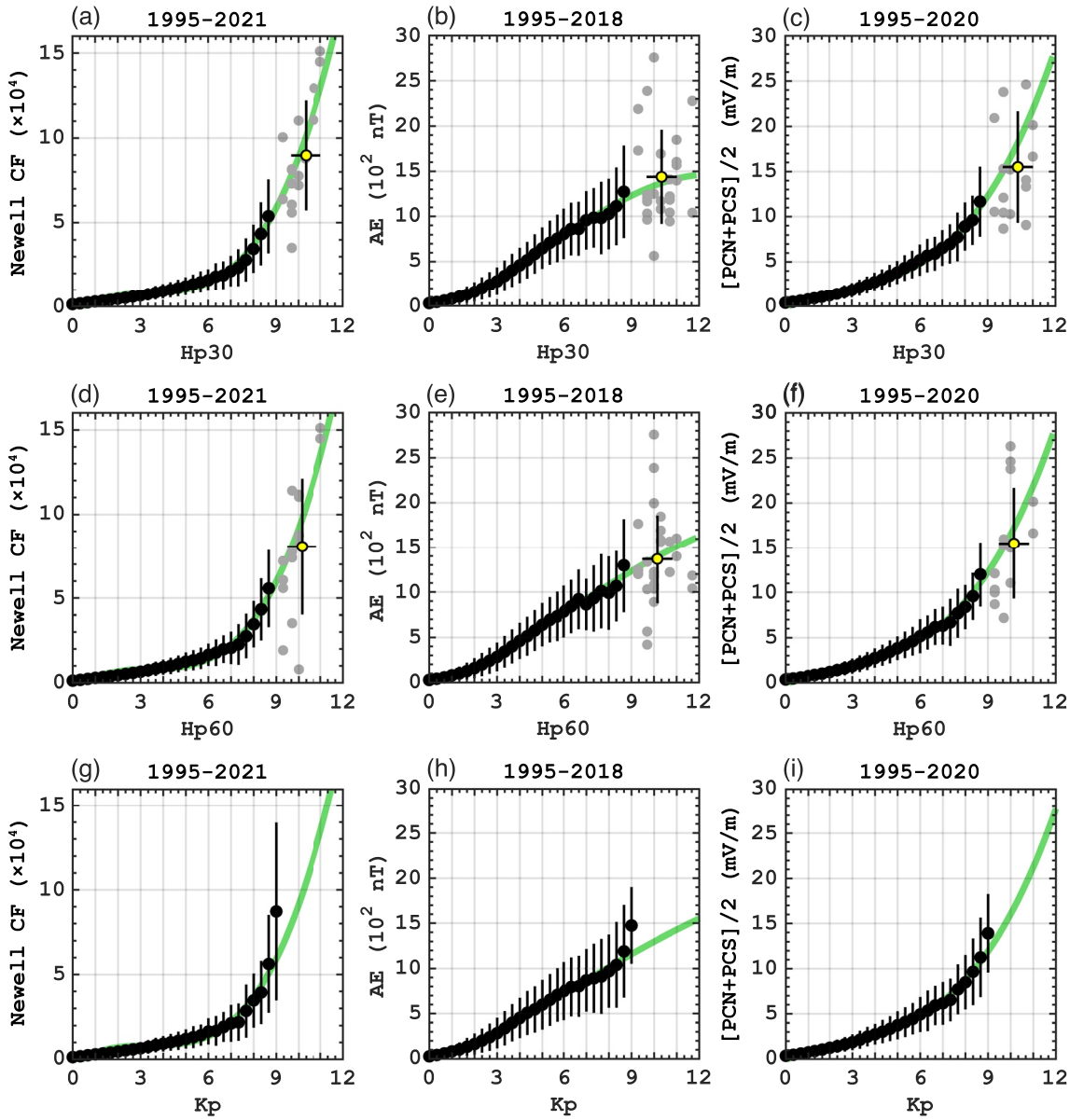

Figure 2. Dependence of (a–c) Hp30, (d–f) Hp60, and (g–i) *Kp* on (a, d, g) Newell's solar-wind coupling function, (b, e, h) AE index, and (c, f, i) PC index. For the PC index, the average of the northern (PCN) and southern (PCS) indices is used, considering only their positive values. In each panel, black dots indicate the average of the solar-wind coupling function, AE or PC index at each Hpo or *Kp* value (0o, 0+, 1−, …, 9−), with error bars representing the standard deviation and the green curve representing the best-fitting third-order polynomial function for Hpo or *Kp* below 9o. The gray dots in panels (a–f) are individual data points for Hpo ≥9o, and the yellow dot is their average value.

To provide some insight into variations of Hp30 and Hp60 within 3 hr, Figure 4 depicts the response of ap30, ap60, and *ap* to isolated substorms. The substorm onset list based on the technique described by Newell and Gjerloev (2011a) was obtained from the SuperMAG website (https://supermag.jhuapl.edu/). We selected isolated substorm events where there is no other substorm onset in the preceding 6 hr and following 12 hr. A total of 1947 isolated substorm events have been identified during 1995–2018. Figure 4a shows the variation of the AE index averaged over those substorm events. The average AE index peaks approximately 1 hr after the onset, and decays gradually to go back to the pre-onset level in 3–4 hr. The average ap30 and ap60 indices (Figures 4b and 4c) show the increase and decrease of geomagnetic activity that occur within 3 hr around the substorm onset. *ap* (Figure 4d) is not able to fully resolve such a short-term variation due to its low time resolution. The results suggest that variation of Hpo within 3 hr can contain physically meaningful information, which is not resolved by *Kp*.

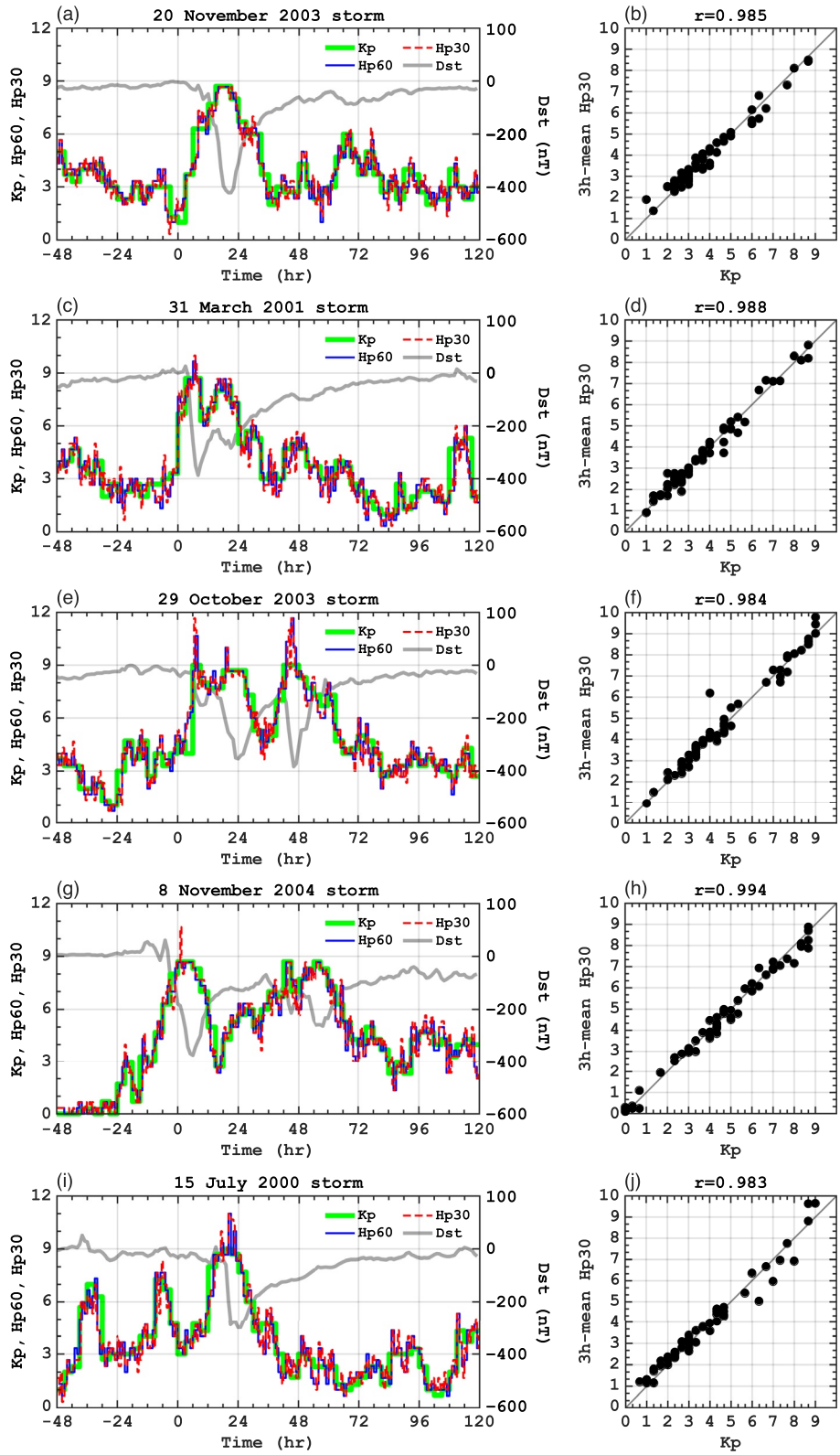

Figure 3. (a, c, e, g, i) Time series of *Kp*, Hp60, Hp30, and Dst over a 7-day interval during strong geomagnetic storm events. Zero in the horizontal axis corresponds to 00 UT of the day with the storm main phase. (b, d, f, h, j) Comparison of *Kp* and three-hourly average of Hp30 during the strong geomagnetic storm events. The 3-hourly average of Hp30 is derived from the corresponding values of ap30. The correlation coefficient *r* is also indicated.

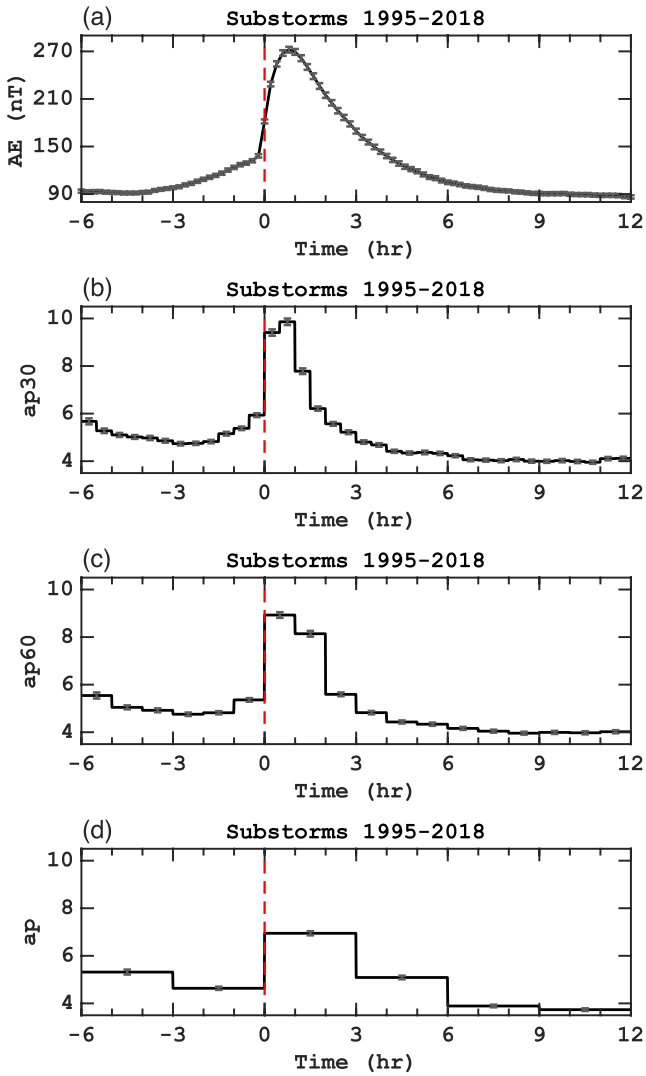

Figure 4. Superposed epoch analysis of (a) AE, (b) ap30, (c) ap60, and (d) *Kp* over 1947 isolated substorm events identified during 1995–2018 based on the method of Newell and Gjerloev (2011a). Error bars represent the standard error of the mean. Zero in the horizontal axis corresponds to the substorm onset.

4. Summary and Outlook

We have described a group of new open-ended geomagnetic activity indices Hpo. Hourly (Hp60) and half-hourly (Hp30) indices, along with their linearly scaled counterparts (ap30 and ap60), are available in near real time from the GFZ website (https://www.gfz-potsdam.de/en/hpo-index) with DOI (Matzka et al., 2022). Important properties of Hpo that are revealed by our initial analysis can be summarized as follows:

1. The frequency distributions of the occurrence of Hp30 and Hp60 values are consistent with that of *Kp* at different phases of the solar cycle (Figures 1a–1i).
2. Month-to-month variations of Hp30 and Hp60 are consistent with that of *Kp* (Figure 1k).
3. The relationships between Hpo indices and Newell's solar wind coupling function, AE and PC indices are similar to those between *Kp* and these three quantities.
4. Hp30 and Hp60 can capture temporal variation of *Kp* during strong geomagnetic storm events (Figure 3).
5. Hp30 and Hp60 can reproduce short-term variation of geomagnetic activity within 3 hr associated with substorms (Figure 4).

These results demonstrate that Hpo can be used as a higher time-resolution alternative to *Kp*. Indeed, there are already a few studies that utilized Hpo for its advantage over *Kp*. Yamazaki et al. (2021) used Hp30 to select quiet-time measurements of the geomagnetic field from Swarm satellites. The orbital period of a Swarm satellite is approximately 90 min, thus using Hp30, geomagnetic activity can be evaluated for every one third of the orbit, while there is only one *Kp* value for every two orbits. The high-cadence output of Hpo enables a more accurate selection of quiet-time data than the three-hourly *Kp* index. Bruinsma and Boniface (2021) used Hp60 to drive a recent version of the Drag Temperature Model, DTM-2020, which is a semi-empirical model of the Earth's thermosphere, developed for orbit determination and prediction of spacecraft and debris. They showed that the use of Hpo leads to the improvement of the model compared with the predecessor model DTM-2013 (Bruinsma, 2015) that is driven by *Kp*. Similarly, Hpo may be used for improving other geospace models driven by *Kp*. Recalibration and validation are recommended when Hpo is used as an input for existing models that are parameterized with *Kp*.

Data Availability Statement

Hpo and apo indices (Hp30, Hp60, ap30, and ap60) are available from the GFZ website (https://www.gfz-potsdam.de/en/hpo-index); see Matzka et al. (2022) for data publication. *Kp* and *ap* indices are also available from the GFZ website (https://www.gfz-potsdam.de/en/kp-index/); and see Matzka, Bronkalla, et al. (2021) for data publication. The sunspot number data are provide by the World Data Center SILSO, Royal Observatory of Belgium, Brussels, and can be downloaded from their website (https://wwwbis.sidc.be/silso/datafiles). The 5-min solar wind data are available from the OMNIWeb (https://omniweb.gsfc.nasa.gov/form/omni_min.html); see also Papitashvili and King (2022). AE and Dst indices are provided by the World Data Center (WDC) for Geomagnetism, Kyoto, and are available at http://wdc.kugi.kyoto-u.ac.jp/dstae/index.html. PCN and PCS indices are provided by the Arctic and Antarctic Research Institute and Technical University of Denmark/DTU Space, and can be obtained from the PC index website (https://pcindex.org/archive). The substorm list is available from the SuperMAG website (https://supermag.jhuapl.edu/substorms/).

Acknowledgments
The authors thank the institutions operating the geomagnetic observatories that contribute near real-time data for the calculation of Hpo and the staff that looks after these observatories. Especially, the authors thank Orsi Baillie, Ellen Clarke, and Sarah Reay from the British Geological Survey for Lerwick (LER) and Eskdalemuir (ESK) data, Charles Blais and David Calp from the Natural Resources Canada for Ottawa (OTT) and Meanook (MEA) data, Abram Claycomb, Jake Morris, and Bill Worthington from the U.S. Geological Survey for Frederiksburg (FRD) and Sitka (SIT) data, Jürgen Haseloff and Katrin Tornow from the GFZ German Research Center for Geosciences for Niemegk (NGK) and Wingst (WNG) data, Andrew Lewis from the Geoscience Australia for Canberra (CNB) data, Tania Petersen from the GNS Science for Eyrewell (EYR) data, Gerhard Schwarz from the Geological Survey of Sweden for Uppsala (UPS) data, and Anna Naemi Willer from the Technical University of Denmark for Brorfelde (BFE) data. Hpo indices were developed as part of the Space Weather Atmosphere Models and Indices project SWAMI (http://swami-h2020.eu/). The SWAMI project has received funding from the European Union's Horizon 2020 Research and Innovation Program under Grant Agreement No. 776287. The authors acknowledge use of NASA/GSFC's Space Physics Data Facility's OMNIWeb service, and OMNI data. The authors acknowledge the substorm timing list identified by the Newell and Gjerloev technique (Newell & Gjerloev, 2011a); the SMU and SML indices (Newell & Gjerloev, 2011b); and the SuperMAG collaboration (Gjerloev, 2012). Open access funding was enabled and organized by Projekt DEAL.

References

Araki, T. (1994). A physical model of the geomagnetic sudden commencement. *Geophysical Monograph-American Geophysical Union*, *81*, 183–200. https://doi.org/10.1029/gm081p0183

Bartels, J., Heck, N., & Johnston, H. (1939). The three-hour-range index measuring geomagnetic activity. *Terrestrial Magnetism and Atmospheric Electricity*, *44*(4), 411–454. https://doi.org/10.1029/te044i004p00411

Bruinsma, S. (2015). The DTM-2013 thermosphere model. *Journal of Space Weather and Space Climate*, *5*, A1. https://doi.org/10.1051/swsc/2015001

Bruinsma, S., & Boniface, C. (2021). The operational and research DTM-2020 thermosphere models. *Journal of Space Weather and Space Climate*, *11*, 47–1. https://doi.org/10.1051/swsc/2021032

Chapman, S., & Bartels, J. (1940). *Geomagnetism*. Oxford University Press.

Drob, D. P., Emmert, J. T., Meriwether, J. W., Makela, J. J., Doornbos, E., Conde, M., et al. (2015). An update to the Horizontal Wind Model (HWM): The quiet time thermosphere. *Earth and Space Science*, *2*(7), 301–319. https://doi.org/10.1002/2014ea000089

Emmert, J. T., Drob, D. P., Picone, J. M., Siskind, D. E., Jones, M., Jr., Mlynczak, M., et al. (2021). NRLMSIS 2.0: A whole-atmosphere empirical model of temperature and neutral species densities. *Earth and Space Science*, *8*(3), e2020EA001321. https://doi.org/10.1029/2020ea001321

Fejer, B. G., Jensen, J. W., & Su, S.-Y. (2008). Quiet time equatorial *F* region vertical plasma drift model derived from ROCSAT-1 observations. *Journal of Geophysical Research*, *113*(A5). https://doi.org/10.1029/2007ja012801

Gjerloev, J. (2012). The SuperMAG data processing technique. *Journal of Geophysical Research*, *117*(A9). https://doi.org/10.1029/2012ja017683

Gonzalez, W., Joselyn, J.-A., Kamide, Y., Kroehl, H. W., Rostoker, G., Tsurutani, B., & Vasyliunas, V. (1994). What is a geomagnetic storm? *Journal of Geophysical Research*, *99*(A4), 5771–5792. https://doi.org/10.1029/93ja02867

Jackson, D. R., Bruinsma, S., Negrin, S., Stolle, C., Budd, C. J., Gonzalez, R. D., et al. (2020). The Space Weather Atmosphere Models and Indices (SWAMI) project: Overview and first results. *Journal of Space Weather and Space Climate*, *10*, 18. https://doi.org/10.1051/swsc/2020019

King, J., & Papitashvili, N. (2005). Solar wind spatial scales in and comparisons of hourly Wind and ACE plasma and magnetic field data. *Journal of Geophysical Research*, *110*(A2), A02104. https://doi.org/10.1029/2004ja010649

Liu, H.-L., Bardeen, C. G., Foster, B. T., Lauritzen, P., Liu, J., Lu, G., et al. (2018). Development and validation of the Whole Atmosphere Community Climate Model with thermosphere and ionosphere extension (WACCM-X 2.0). *Journal of Advances in Modeling Earth Systems*, *10*(2), 381–402. https://doi.org/10.1002/2017ms001232

Lockwood, M., Stamper, R., & Wild, M. (1999). A doubling of the Sun's coronal magnetic field during the past 100 years. *Nature*, *399*(6735), 437–439. https://doi.org/10.1038/20867

Lyons, L. (1996). Substorms: Fundamental observational features, distinction from other disturbances, and external triggering. *Journal of Geophysical Research*, *101*(A6), 13011–13025. https://doi.org/10.1029/95ja01987

Manoj, C., Maus, S., Lühr, H., & Alken, P. (2008). Penetration characteristics of the interplanetary electric field to the daytime equatorial ionosphere. *Journal of Geophysical Research*, *113*(A12). https://doi.org/10.1029/2008ja013381

Matzka, J., Bronkalla, O., Kervalishvili, G., Rauberg, J., Stolle, C., & Yamazaki, Y. (2022). Geomagnetic Hpo index. V. 2.0 [Dataset]. GFZ Data Services. Retrieved from https://www.gfz-potsdam.de/en/hpo-index/

Matzka, J., Bronkalla, O., Tornow, K., Elger, K., & Stolle, C. (2021). Geomagnetic Kp index. V. 1.0 [Dataset]. GFZ Data Services. Retrieved from https://www.gfz-potsdam.de/en/kp-index/

Matzka, J., Stolle, C., Yamazaki, Y., Bronkalla, O., & Morschhauser, A. (2021). The geomagnetic *Kp* index and derived indices of geomagnetic activity. *Space Weather*, *19*(5), e2020SW002641. https://doi.org/10.1029/2020sw002641

Mayaud, P. (1980). *Derivation, Meaning and Use of Geomagnetic Indices, Volume 22*. American Geophysical Union.

McPherron, R. L. (1970). Growth phase of magnetospheric substorms. *Journal of Geophysical Research*, *75*(28), 5592–5599. https://doi.org/10.1029/ja075i028p05592

McPherron, R. L. (2005). Magnetic pulsations: Their sources and relation to solar wind and geomagnetic activity. *Surveys in Geophysics*, *26*(5), 545–592. https://doi.org/10.1007/s10712-005-1758-7

Newell, P., & Gjerloev, J. (2011a). Evaluation of SuperMAG auroral electrojet indices as indicators of substorms and auroral power. *Journal of Geophysical Research*, *116*(A12). https://doi.org/10.1029/2011ja016779

Newell, P., & Gjerloev, J. (2011b). Substorm and magnetosphere characteristic scales inferred from the SuperMAG auroral electrojet indices. *Journal of Geophysical Research*, *116*(A12). https://doi.org/10.1029/2011ja016936

Newell, P. T., Sotirelis, T., Liou, K., Meng, C.-I., & Rich, F. J. (2007). A nearly universal solar wind-magnetosphere coupling function inferred from 10 magnetospheric state variables. *Journal of Geophysical Research*, *112*, A01206. https://doi.org/10.1029/2006JA012015

Papitashvili, N. E., & King, J. H. (2022). OMNI 5-min data set [Dataset]. NASA Space Physics Data Facility. https://doi.org/10.48322/gbpg-5r77

Saito, T. (1969). Geomagnetic pulsations. *Space Science Reviews*, *10*(3), 319–412. https://doi.org/10.1007/bf00203620

Shprits, Y., Subbotin, D., Ni, B., Horne, R., Baker, D., & Cruce, P. (2011). Profound change of the near-Earth radiation environment caused by solar superstorms. *Space Weather*, *9*(8). https://doi.org/10.1029/2011sw000662

Shprits, Y., Vasile, R., & Zhelavskaya, I. S. (2019). Nowcasting and predicting the *Kp* index using historical values and real-time observations. *Space Weather*, *17*(8), 1219–1229. https://doi.org/10.1029/2018sw002141

Stauning, P. (2007). A new index for the interplanetary merging electric field and geomagnetic activity: Application of the unified polar cap indices. *Space Weather*, *5*(9). https://doi.org/10.1029/2007sw000311

Subbotin, D., Shprits, Y., & Ni, B. (2011). Long-term radiation belt simulation with the VERB 3-D code: Comparison with CRRES observations. *Journal of Geophysical Research*, *116*(A12). https://doi.org/10.1029/2011ja017019

Sucksdorff, C., Pirjola, R., & Häkkinen, L. (1991). Computer production of K-indices based on linear elimination. *Geophysical Transactions*, *36*, 333–345.

Thomsen, M. (2004). Why *Kp* is such a good measure of magnetospheric convection. *Space Weather*, 2(11). https://doi.org/10.1029/2004sw000089

Troshichev, O., Andrezen, V., Vennerstrøm, S., & Friis-Christensen, E. (1988). Magnetic activity in the polar cap – A new index. *Planetary and Space Science*, *36*(11), 1095–1102. https://doi.org/10.1016/0032-0633(88)90063-3

Vallado, D. A., & Finkleman, D. (2014). A critical assessment of satellite drag and atmospheric density modeling. *Acta Astronautica*, *95*, 141–165. https://doi.org/10.1016/j.actaastro.2013.10.005

Yamazaki, Y., Harding, B., Stolle, C., & Matzka, J. (2021). Neutral wind profiles during periods of eastward and westward equatorial electrojet. *Geophysical Research Letters*, *48*(11), e2021GL093567. https://doi.org/10.1029/2021gl093567

Yamazaki, Y., & Maute, A. (2017). Sq and EEJ–A review on the daily variation of the geomagnetic field caused by ionospheric dynamo currents. *Space Science Reviews*, *206*(1), 299–405. https://doi.org/10.1007/s11214-016-0282-z